THE JOURNAL OF PHYSICAL CHEMISTRY C
A JOURNAL OF THE AMERICAN CHEMICAL SOCIETY

pubs.acs.org/JPCC

Article

Influence of Support Physicochemical Properties on the Oxygen Evolution Reaction Performance of ITO-Supported IrO_x Nanoparticles

Published as part of the The Journal of Physical Chemistry virtual special issue "Early-Career and Emerging Researchers in Physical Chemistry Volume 2".

Julie-Ann Hoffman, Ziba S. H. S. Rajan, Darija Susac, Mangaka C. Matoetoe, and Rhiyaad Mohamed*

Cite This: *J. Phys. Chem. C* 2023, 127, 894–906

Read Online

ACCESS | Metrics & More | Article Recommendations | Supporting Information

ABSTRACT: The widespread implementation of proton exchange membrane water electrolyzers (PEMWEs) is greatly hindered by the availability and high costs associated with key catalyst and electrode components. The anodic oxygen evolution reaction (OER) is known to be kinetically challenging and therefore requires substantially high loadings of Ir-based catalysts (~2 mg cm^{-2}). A promising strategy to lower the amount of iridium is to enhance the electrocatalytically active surface area, by means of dispersing finely divided nanoparticles of iridium/iridium oxide over cheaper, electronically conductive, stable oxide support materials. In this work, we use a metal−organic chemical deposition (MOCD) technique to deposit IrO_x (x = 0−2) nanoparticles on tin-doped indium oxide (ITO) supports with different physicochemical properties such as specific surface area and Sn dopant concentration. The MOCD technique has been proven to deliver catalysts with well-dispersed nanoparticles and narrow particle size distributions. This approach, in combination with the chosen ITO supports, allows for decoupling of particle size and Ir loading effects from other catalyst−support interactions that are contributing to catalyst activity, stability, and nature of deposited nanoparticles. In this way, we were able to investigate the effect of IrO_x nanoparticle coverage effects on ITO and found that high nanoparticle coverage, i.e., low interparticle distances of the IrO_x nanoparticles supported on low surface area ITO, increased the stability of the support. The specific surface area of ITO supports was found to correlate with the nature of surface Sn and In species, which in turn influenced the nature of deposited IrO_x nanoparticles for enhanced OER activity. The most stable OER catalyst had highly dispersed, small (2.4 ± 0.7 nm), predominantly metallic Ir nanoparticles with a high mass-specific OER activity of 207 ± 34 A g_{Ir}^{-1} at 1.525 V vs RHE. This was obtained by the interplay of the Ir phase, optimized for improved activity and low interparticle distance for catalyst stability.

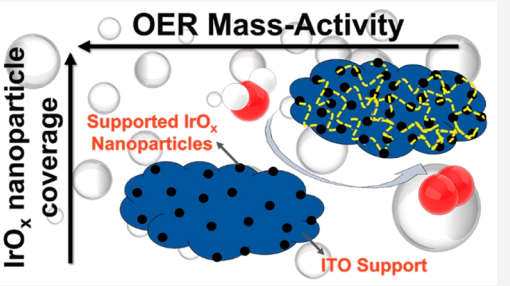

1. INTRODUCTION

In the past few years, the adverse consequences of climate change have been exacerbated at an alarming rate, propelling the scientific community toward the pursuit of innovative technological solutions to pave the way for a sustainable, net-zero future. One of the most promising energy vectors in this future energy landscape is hydrogen. Hydrogen is a versatile energy carrier currently produced predominantly by the processing of carbon-based fossil fuels. Coupled with renewable electricity such as solar or wind energy, proton exchange membrane electrolyzers (PEMWEs) offer a host of advantages for the generation of green hydrogen at competitive market prices <2€/kg of H_2.[1,2] PEMWEs are capable of achieving high current densities (above 2 A cm^{-2}), while simultaneously offering a compact design, the ability for fast start-up and shut-down, and the production of high-purity hydrogen with a minimal carbon footprint. However, further innovation and reductions in electrolyzer component cost for large-scale production of green hydrogen are still required.[3,4]

The current state-of-the-art PEMWE technology makes use of rare, platinum group metals (PGMs) as catalysts for the oxygen and hydrogen evolution reactions.[5−7] The anodic oxygen evolution reaction (OER) is considered to be the bottleneck of the water electrolysis process, as a consequence of its slow reaction kinetics, which demand vast quantities of PGMs for efficient, feasible electrolyzer operation. The high overpotential to be overcome by such catalysts greatly limits

Received: September 12, 2022
Revised: December 13, 2022
Published: January 9, 2023

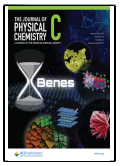

https://doi.org/10.1021/acs.jpcc.2c06501
J. Phys. Chem. C 2023, 127, 894−906

Table 1. Summary of Physical Properties of the ITO Supports

	ICP-OES measurements[a]		SEM-EDX measurements[a]			
sample id	In (wt %)	Sn (wt %)	In (wt %)	Sn (wt %)	estimated crystallite size (nm)	average specific surface area (SSA) ($m^2\ g^{-1}$)
ITO-A	95.0 ± 0.5	5.0 ± 0.1	94.0 ± 2.3	6.0 ± 1.8	18.6	29.0
ITO-B	95.0 ± 0.4	5.0 ± 0.1	95.0 ± 1.7	5.0 ± 1.5	31.9	10.0
ITO-C	90.0 ± 0.4	10.0 ± 0.1	90.0 ± 1.7	10.0 ± 1.4	17.2	32.0
ITO-D	90.0 ± 0.1	10.0 ± 0.1	90.0 ± 1.8	10.0 ± 1.5	30.9	10.0

[a]With standard deviation shown.

the choice of materials that can be employed in PEMWE devices. These materials need to demonstrate sufficient catalytic activity and be stable under the harsh, severely oxidizing conditions of the OER.[6,8,9] Iridium oxide (IrO_2) is seen as the most promising OER electrocatalyst due to its ability to offer the necessary compromise of high activity and adequate corrosion resistance.[10−12] Nevertheless, the high cost and scarcity of iridium greatly limits the scale-up and widespread commercialization of PEMWE technology.[5,11,13−15]

These challenges can be addressed by the development of supported electrocatalysts, where a substantial reduction of Ir content and increase in catalyst utilization is realized by finely dividing iridium nanoparticles over a suitable support material, as a means to enhance the electrocatalytically active surface area.[16−19] In addition to significant cost reductions by lowering Ir metal loadings, several structure−property−function relationships between the catalytically active phase and the support have been reported to have positive effects on the operational lifetime of the supported electrocatalysts.[20−22] To exploit these advantages, it is generally accepted that support materials require chemical and electrochemical stability in the OER environment, be high-surface-area materials capable of forming porous layers, and finally, offer sufficient electronic conductivity. Doped oxide support materials such as antimony-doped tin oxide (ATO), tin-doped indium oxide (ITO), and fluorine-doped tin oxide (FTO) have demonstrated considerably improved electronic conductivities compared to those of their undoped oxide counterparts.[23−25] The use of these supports resulted in fine dispersions of IrO_x nanoparticles, which significantly enhanced the electrocatalytically active surface areas of these catalysts and consequently improved their OER performance.[17,18,23−30] However, the nature of the improved performance is not well understood and merits the need for a systematic study of the various interactions between the Ir phase and the support material.

In this regard, the use of ITO is quite interesting. ITO predominantly consists of indium oxide (In_2O_3) and is predicted to be neither chemically or electrochemically stable in acid and under OER conditions. Some studies[31−34] have reported indium dissolution in the OER potential window in acidic media, claiming that the stability of ITO hinders its ability to perform well as an OER support material. Geiger et al.[33] found that ITO was unstable even at open circuit potentials due to the dissolution of In, resulting in a loss of conductivity, thereby suggesting that ITO is not suitable for use as an OER support. The authors also subsequently found no benefit to using ITO as an OER support material, questioning the use of doped-oxide supports for the OER in its entirety.[31] However, a study by Oh, Nong, and Strasser[24] reported the preparation of mesoporous high-surface-area ITO (9 at. % Sn) powders (125 $m^2\ g^{-1}$) with 2 orders of magnitude increased electrical conductivity compared to that of undoped SnO_2 and found that the electrochemical stability was increased compared to that of carbon black, when cycled between 0.40 and 1.40 V vs RHE for up to 10000 cycles. Furthermore, satisfactory OER performance in terms of both activity and stability for ITO-supported iridium-based electrocatalysts was reported by several authors. In these studies, the morphology of the IrO_x phase varied widely, from atomically dispersed Ir with a low Ir loading (0.86 wt %)[30] to IrO_x layers[34] and IrO_x nanoparticles with up to relatively high Ir loadings (90 wt %).[17,29,31] For example, Delgado et al.[28] stated that their best performing catalyst was 30 wt % IrO_2/ITO with ≈176 A g_{Ir}^{-1} at 1.51 V vs RHE (*iR*-corrected). This catalyst showed a small decrease in mass-specific OER activity after a 2 h stability test (to reach overpotential of 10 mA cm^{-2}). As such, the literature on the use of ITO as an OER support is disparate and its viability for PEMWE applications remains questionable. In addition, the OER stability measurements in the aforementioned studies were performed via application of different electrochemical techniques, which complicates the understanding of the origin of the observed disparities.

In this study, the effect of the physicochemical properties of the ITO support on the OER performance of IrO_x nanoparticles supported thereon was investigated. In our previous work, a simple, robust, metal−organic chemical deposition (MOCD) technique demonstrated its effectiveness for the deposition of small, highly dispersed Pt and IrO_2 nanoparticles with narrow particle size distributions on various support materials with well-controlled metal loadings.[27,35−38] In this work, the MOCD method has been extended to deposit small IrO_x nanoparticles on a selection of ITO supports with various specific surface areas (SSAs) and Sn:In weight ratios. In this way, the influence of the nanoparticle coverage and in turn the interparticle distance of the IrO_x nanoparticles could be investigated, while excluding particle size and Ir metal loading effects for the IrO_x phase.

The physicochemical properties of the supports and the IrO_x/ITO catalyst counterparts were characterized by X-ray diffraction (XRD), scanning electron microscopy-energy dispersive X-ray spectroscopy (SEM-EDX), high-resolution scanning transmission electron microscopy (HR-STEM), X-ray photoelectron spectroscopy (XPS), and inductively coupled plasma-optical emission spectroscopy (ICP-OES). The activity and stability of these electrocatalysts toward the oxygen evolution reaction was investigated using an *ex-situ* three-electrode system with a rotating disk electrode (RDE) setup in acidic media. This work demonstrates that the nature of the iridium phase and the extent of IrO_x coverage over the ITO support has a stabilizing effect on the prepared electrocatalysts under OER conditions.

https://doi.org/10.1021/acs.jpcc.2c06501
J. Phys. Chem. C 2023, 127, 894−906

2. EXPERIMENTAL METHODS

2.1. Preparation of IrO_x/ITO by Metal−Organic Chemical Deposition. Iridium *tris*-acetylacetonate, $Ir(acac)_3$ (Sigma-Aldrich, 97% purity), was used as the Ir source for supported catalyst preparation. Four different commercially available ITO nanopowder support materials (US Research Nanomaterials Inc., 99.99+% purity), with varying In_2O_3:SnO_2 (95:5 or 90:10 wt %) and varying average particle size (small (14 nm) and large (up to 75 nm)) were used as received to make all the IrO_x/ITO catalysts (see Table 1). The IrO_x/ITO catalysts were prepared to have a nominal 20 wt % iridium mass loading by the MOCD method, as described in our previous publication.[27] Briefly, the deposition process involves grinding together the metal−organic precursor, $Ir(acac)_3$, and the ITO support. This mixture is then placed into a stainless reactor vessel and calcined in a tubular furnace at 320 °C for 2 h in an oxidizing environment.

2.2. Physical Characterization. X-ray diffraction (XRD) was carried out on a Bruker D8 Advance diffractometer operating at 40 kV with a Co Kα radiation source ($k_{\alpha 1}$ = 0.178897 nm). This technique was used to verify the structure of the ITO support materials and MOCD IrO_x/ITO catalysts.

Transmission electron microscopy (TEM) (bright field imaging) was performed using a FEI TECNAI F20 FEGTEM microscope operated at 200 kV. Normalization of the particle size distribution was achieved by using the measurement of Ferret diameter from 300 nanoparticles using ImageJ software. An FEI TEM Osiris microscope operated at 200 kV in a STEM mode with ChemiSTEM energy dispersive X-ray (EDX) detector system was used to obtain high-resolution scanning transmission microscopy (HR-STEM) and elemental maps for supported catalysts. Bruker Esprit software was used to process the acquired maps.

Brunauer−Emmett−Teller (BET) physisorption measurements were carried out to determine the specific surface area (SSA) of the ITO support materials using a Micromeritics Tristar II Series instrument, which had a range from 0 to 950 mmHg. All results were analyzed using Micromeritics TriStar II 3020 Version 2.00 software.

A Varian ES 730 ICP-OES was used to perform inductively coupled plasma-optical emission spectrometry (ICP-OES) measurements for the quantitation of dissolved Sn and In species in the commercial ITO support materials. Prior to analysis, a Mars 6 Microwave Digester was used to digest the samples.

SEM-EDX measurements were used in this work for the quantitation of the elements in the commercial ITO support materials as well as for the determination of the iridium mass loadings of the MOCD IrO_x/ITO catalysts. These measurements were performed on an FEI Nova NanoSEM 230 operating at 20 kV beam energy and equipped with an Oxford X-Max X-ray detector. INCA Point & ID software was used to analyze the X-ray spectra and quantify the elements.

X-ray photoelectron spectroscopy (XPS) measurements were performed on a Kratos Analytical Axis Ultra DLD system together with a monochromated Al Kα source (1486.71 eV). The instrument was calibrated using Au 4f at 84.0 eV. For catalyst samples (IrO_x on ITO), C 1s was measured at 285 eV. Spectra from ITO supports were calibrated with respect to C 1s at 285.0 eV. High-resolution spectra were obtained using 20 eV pass energy. XPSPeak4.1 software was utilized for fitting of the Ir 4f, In 3d, Sn 3d, and O 1s components. For all photoelectron peaks, a Lorentzian/Gaussian ratio of 20 and TS and TL asymmetry factors of 0.2 and 100 were used for curve-fitting of the spectra, unless stated otherwise. For In 3d and Sn 3d spectra, the subcomponent analysis approach was similar to that in published papers by Detweiler et al.,[39] Donley et al.[40] and Teterin et al.[41] For the Ir 4f spectrum, curve-fitting was done following an approach taken by Rajan et al.,[27] which was in agreement with works by Pfeifer et al.[42] and Yu et al.[43] The Ir $4f_{7/2}$ doublet component from Ir(0), Ir(IV), and Ir(III) was identified at 60.8, 61.5, and 62.4 eV, respectively. Satellite peaks (Ir $4f_{7/2}$) for Ir(IV) were identified at 62.8 and 67.8 eV and for Ir(III) at 63.3 eV. The O 1s spectrum had all oxygen components fitted with a FWHM of 1.38 eV, and TS and TL asymmetry factors of 0.1 and 100 were implemented for oxygen bonded to metallic components, while asymmetry factors of 0 and 1 were implemented for oxygen bonded to carbon components.

2.3. Electrochemical Characterization. Catalysts inks were prepared with 10 mg of catalyst, 20 μL of 5 wt % Nafion (Nafion 117, Merck), and 5 mL of solvent. The solvent for IrO_x/ITO catalysts was made up of 4 mL of ethanol and 1 mL of water. Two commercial benchmarks, IrO_2−TiO_2 (Elyst Ir75) and Ir black (Umicore AG & Co. KG), were utilized to compare the OER performances of the MOCD IrO_x/ITO catalysts. For the commercial materials, the catalyst inks consisted of 1 mL of isopropanol and 4 mL of water. The inks were homogenized via ultrasonication for 30 min, after which they were magnetically stirred at 400 rpm as the ink was drop-cast onto the working electrodes, consisting of glassy carbon (surface area of 0.196 cm^2). To achieve similar iridium mass loadings on the working electrodes, 10 and 40 μL of the commercial catalysts and the MOCD IrO_x/ITO inks were deposited, respectively. All electrodes were dried in ambient conditions. The electrochemical characterization was performed in a single compartment three-electrode cell (150 mL glass cell, PINE Research), using a rotating disk electrode (RDE) setup[44] and a Bio-Logic SP-300 double-channelled potentiostat, equipped with EC-Lab V11.20 software. Prior to electrochemical measurements, the Hg/Hg_2SO_4 reference electrode was calibrated in H_2 saturated 0.1 M $HClO_4$ (Suprapur, Merck) electrolyte with a flame sterilized platinum wire acting as the counter electrode. The measurements were taken in O_2 saturated 0.1 M $HClO_4$ electrolyte at room temperature. To encourage the removal of evolved O_2 gas bubbles,[5,45,46] the RDE setup was set to rotate the working electrode at 1600 rpm and the RDE setup stand was tilted by 15−30°.

Cyclic voltammetry was performed on all working electrodes to remove surface contaminants and activate the catalyst layer. The electrochemical cleaning and activation cycles were done with 10 cycles and a scan rate of 50 mV s^{-1}, followed by 10 cycles at a scan rate of 10 mV s^{-1} in the potential range 1.0−1.40 V vs RHE. Chronoamperometry (CA) was then used to measure the OER activity and stability. For the OER activity evaluation, initial activation CA steps from 1.40 to 1.48 V vs RHE with 1 min hold at each step were applied and, thereafter, OER activity determination steps from 1.50 to 1.56 V vs RHE with 1 min hold at each step were used. The stability determination test was done by applying the OER activity CA steps before and after holding the potential at 1.60 V vs RHE for 2 h in order to derive the relative mass activity loss of the catalysts. Lastly, the ohmic resistance utilized for *iR*-correction of the specific mass OER activity of catalysts was determined

https://doi.org/10.1021/acs.jpcc.2c06501
J. Phys. Chem. C 2023, 127, 894−906

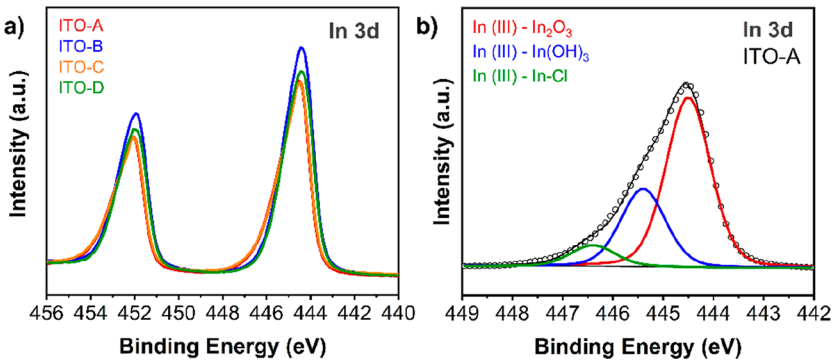

Figure 1. (a) In 3d XPS spectra for all ITO supports and (b) an example of a curve fitted In $3d_{5/2}$ for ITO-A.

from electrochemical impedance spectroscopy (EIS). Normalization of data by the iridium mass loading was determined from the SEM-EDX characterization. Three working electrodes were prepared to evaluate the OER performance for each catalyst to ensure reproducibility and reliability of results. The corresponding standard deviation across three electrochemical performance evaluations was then used to compute the error.

3. RESULTS AND DISCUSSION

3.1. Physical Characterization of ITO Supports. To enable the investigation of the effect of nature of the ITO support on the nature of supported catalyst, ITO support materials with varying dopant concentration and specific surface areas (SSA) and crystallite sizes were selected. Table 1 summarizes the differences in the four ITO supports that were used for the catalyst preparation.

Tin dopant concentrations of 5 wt % (ITO-A and ITO-B) and 10 wt % (ITO-C and ITO-D) were confirmed by ICP-OES and SEM-EDX measurements. Smaller crystallite sizes, as calculated by the Debye−Scherrer equation from the XRD patterns (see Figure S1 in the Supporting Information), were observed for ITO-A and ITO-C compared to results for ITO-B and ITO-D. This corresponded to average SSA values of the ITO supports that varied from a low SSA of 10 m^2g^{-1} (ITO-B and ITO-D) to 3 times higher SSA values of 29−32 m^2g^{-1} (ITO-A and ITO-C).

XPS measurements were performed on the ITO supports to gain an understanding of the phases present at their surfaces. From quantitative analysis of the low-resolution survey spectra (see Table S3 in the Supporting Information), larger values for Sn/In wt % ratios were measured from all ITO supports compared to the corresponding bulk ratios from ICP-OES, indicating that the Sn appears to be enriched at the surface relative to In.

Figure 1a illustrates the high-resolution XPS spectra of In 3d measured from four ITO supports. The In $3d_{5/2}$ and In $3d_{3/2}$ at corresponding binding energies of 444.5 and 452.1 eV overlap for all samples indicating similar natures for In species. A representative example for the curve fitted In $3d_{5/2}$ is shown in Figure 1b for ITO-A. The dominant component at binding energy of 444.5 eV is consistent with the presence of In(III) (as expected for In_2O_3) while those shifted to higher binding energies were found to correspond to contributions from $In(OH)_3$ at 445.5 eV and likely due to In bonded to chlorine species at 446.4 eV.[47,48] $In(OH)_3$ most probably occurs due to the hydroxylation on the surface of the ITO due to the disrupted ITO lattice.[40] Indium bonded to chlorine species may have originated from the presence of trace amounts of chlorine as indicated in survey spectra quantification from all supports (see Table S3 in the Supporting Information). This is possibly due to impurities left behind after ITO synthesis. The component percentages shown in Table 2, are seen to vary among ITO supports with average SSA values, where low-SSA supports (ITO-B and ITO-D) have fewer $In(OH)_3$ species on the surface than the high-SSA supports (ITO-A and ITO-C).

Table 2. In 3d and Sn 3d XPS Curve-Fitting Parameters for the ITO Support

			component percentage (%)			
species	binding energy (eV)	FWHM (eV)	ITO-A	ITO-B	ITO-C	ITO-D
In 3d						
In_2O_3	444.5	1.14	63	76	66	75
$In(OH)_3$	445.5	1.14	29	24	27	25
In−Cl	446.4	1.14	8		7	
Sn 3d						
SnO	486.5	1.32	54	56	49	72
SnO_2	487.1	1.32	34	38	40	22
Sn−Cl	488.2	1.32	12	6	11	6

Figure 2a displays the high-resolution XPS spectra of Sn 3d for all the ITO supports. As in the case of In 3d, the Sn 3d spectra are also well aligned, indicating a similar nature of Sn surface species in all supports. For the Sn spectra, the dominant component is Sn(II) (SnO) at 486.5 eV followed by Sn (IV) (SnO_2) at 487.1 eV with a small contribution of Sn bonded to chlorine species, as illustrated in the representative example in Figure 2b) for ITO-A. The presence of SnO and SnO_2 is in agreement with findings of Donley et al.[40] and Teterin et al.,[41] where the presence of SnO may be attributed to imperfections in the ITO lattice structure.

For the O 1s spectra (see Figure S4 in the Supporting Information), the majority contribution (~58−78%) originates from oxygen bonded to metal species (both In and Sn) at the binding energy of 530.3 eV (actual curve-fitting not shown). The clearly visible shoulders at the higher binding energies of 531.8 and 533.2 eV agree well with the presence of metal bonded to hydroxyl groups as well as oxygen associated with hydrocarbon moieties present on the surface, which were also observed from C 1s spectra (see example spectra in Figure S4 in the Supporting Information).

3.2. Physical Characterization of the ITO-Supported IrO_x Electrocatalysts. *Iridium Metal loading.* For IrO_x deposition via the MOCD method, a nominal iridium mass loading of 20 wt % was targeted. However, the SEM-EDX

https://doi.org/10.1021/acs.jpcc.2c06501
J. Phys. Chem. C 2023, 127, 894−906

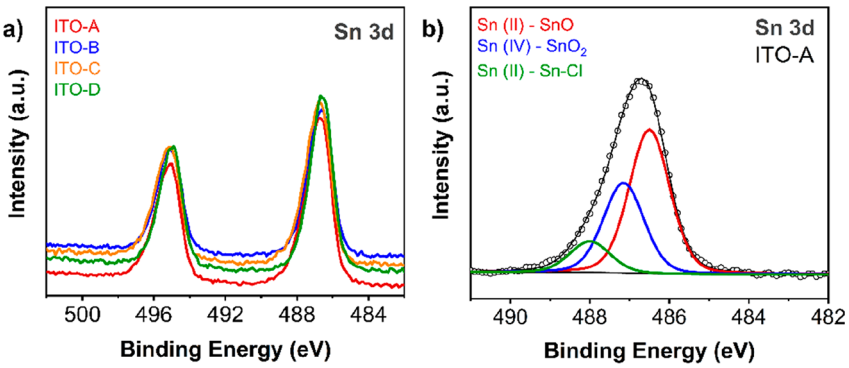

Figure 2. (a) Sn 3d XPS spectra of ITO supports and (b) curve-fitted XPS spectra of ITO-A.

measurements confirmed that values between 8 and 12 wt % were achieved for all catalysts (Table 3). This reduction in actual vs targeted iridium loadings was also observed with an ATO support where such discrepancy was explained as a consequence of the incomplete transfer of Ir species from the precursor to the ATO support due to vaporisation of the Ir precursor.[27]

Table 3. Iridium Mass Loading of the IrO_x/ITO Catalysts as Measured by SEM-EDX

catalyst sample id	ITO support used	Ir loading (wt %)[a]
CAT-A	ITO-A	8.0 ± 0.4
CAT-B	ITO-B	11.0 ± 0.8
CAT-C	ITO-C	12.0 ± 0.5
CAT-D	ITO-D	11.0 ± 0.9

[a]With standard deviation shown.

Structural and Microstructure of the Supported Catalyst. Structural characterization of the prepared catalysts was determined by XRD (see Figure S2 in the Supporting Information). In agreement with previous publications,[27,29] no distinguishable Ir metal and/or IrO_2 features are present in the XRD patterns. This can be explained by the presence of small IrO_x particles below the XRD detection limit (~3 nm).

Figure 3a–f displays representative TEM micrographs of the catalysts, which illustrate the dispersion of IrO_x catalytic nanoparticles over the ITO supports. This confirmed the expected IrO_x nanoparticle coverage differences between catalysts utilizing low-SSA (CAT-B and CAT-D) and high-SSA (CAT-A and CAT-C) supports. Higher nanoparticle coverages are displayed for CAT-B and CAT-D where a low-SSA (10 m^2 g^{-1}) ITO was used. This is supported by the comparison of HR-STEM micrographs for CAT-A and CAT-B (Figure 3e,f). The interparticle distance of IrO_x nanoparticles was estimated using a method outlined by Inaba et al.[49] Values for the interparticle distance are shown in Table S2 of the Supporting Information. For low-SSA supports, the interparticle distance is approximately 4 times larger than for high-SSA supports. The shape of the IrO_x particles supported on the ITO as well as their average nanoparticle size was consistent with the morphology of the particles previously observed for IrO_2 deposited on ATO by the same method.[27] The IrO_x catalytic nanoparticles appear to be spherical in shape and no core–shell structures were identified in the TEM and HR-STEM micrographs. Additionally, all catalysts displayed similar IrO_x particle size distributions (Figure 3a–d), with frequency maxima at ~2.2 nm, although CAT-D has fewer contributions from particles larger than 3 nm compared to results for the other catalysts. Ir and IrO_2 have similar lattice spacings, for which reason it is often difficult to decisively distinguish whether the nanoparticles are of metallic or oxide nature. To illustrate this, measured lattice spacing values for CAT-A are shown in Table S1 and Figure S3 in the Supporting Information. These data indicate the presence of both metallic Ir and IrO_2.

HR-STEM EDX color composite maps for catalysts are displayed in Figure 4a–h. The top row, Figure 4a–d, illustrates the overlap among Ir, In, and Sn components, while the bottom row, Figure 4e–h, focuses on Ir and O distributions. The maps confirm that IrO_x was successfully deposited onto the ITO supports and that the higher nanoparticle coverage was obtained on supports of lower BET surface areas. The Ir and O color composite maps presented in Figure 4e–h suggest that the deposited nanoparticles may be present in a predominantly metallic phase on all catalysts.

Nature and Composition of the Catalysts. From the high-resolution XPS spectra measured from MOCD catalysts (Figure 5a) CAT-A, -B, and -D display similar Ir 4f envelopes, with Ir $4f_{7/2}$ and Ir $4f_{5/2}$ occurring at 61.8 and 64.8 eV, respectively, while the spectrum for CAT-C is shifted 0.7 eV toward higher binding energies. Curve-fitting analysis following previously published approaches[27,42] (Figure 5b,c) revealed that the Ir phase for CAT-A, CAT-B, and CAT-D is present primarily in the metallic form (~52–56%), with secondary contributions from Ir(IV) and minor contributions from Ir(III). In contrast, CAT-C underwent oxidation, with Ir(IV) being the dominant subcomponent (65%), followed by Ir(0) and Ir(III) (Figure 5d). This suggests that in the case of CAT-C, optimum conditions for the formation of predominantly the Ir(IV) component were possibly reached with the combination of small ITO support crystallite sizes and a larger surface Sn dopant content compared to the cases of the other catalysts (see Table S3 in the Supporting Information). This is interesting as all the catalysts were prepared under the same deposition conditions (O_2 environment at 320 °C) as in Rajan et al.,[27] where we reported Ir(IV) as the dominating Ir species on ATO (SnO_2:Sb_2O_3 = 90:10 wt %, approximately 30 nm particle size; 95 m^2 g^{-1} BET surface area). It was seen that the IrO_2 nanoparticles had epitaxially anchored themselves onto the surface of the ATO support. This phenomenon is well explained by the structural similarity between the unit cell parameters of the rutile structures of the SnO_2 phase in the ATO support and those of the iridium oxide phase and is direct proof for the presence of a structural metal–support interaction.[27] However, in the present work, the support

https://doi.org/10.1021/acs.jpcc.2c06501
J. Phys. Chem. C 2023, 127, 894–906

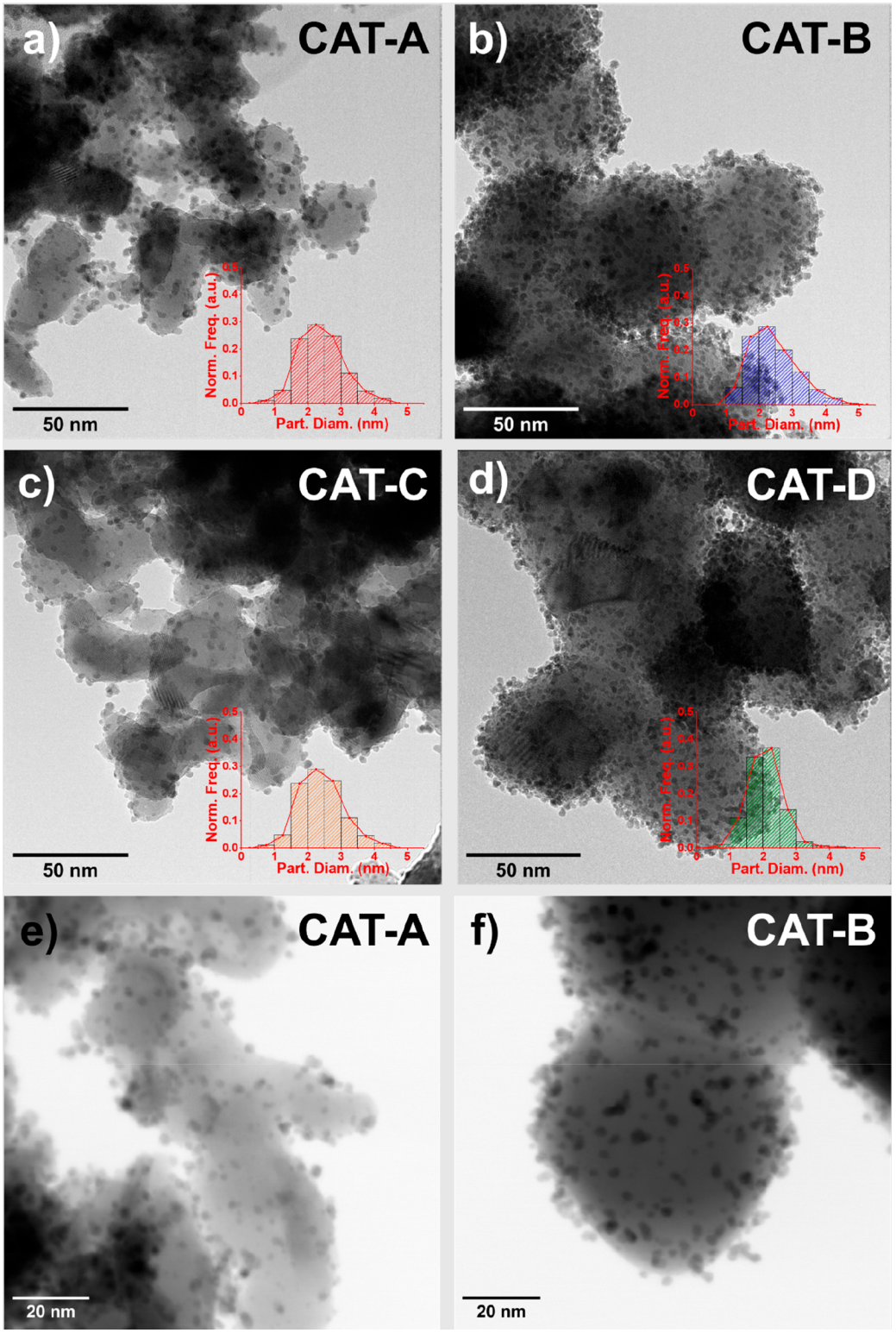

Figure 3. TEM micrographs and particle size distribution (inset) where (a–d) display CAT-A to CAT-D, where Part. Diam. and Norm. Freq refer to particle diameter and normalized frequency, respectively, and (e,f) are high magnification HR-STEM micrographs of CAT-A and CAT-B.

consists of Sn-doped In_2O_3, where metallic iridium was found to be the dominating iridium phase in three out of four synthesized catalysts. In_2O_3 is known to exist in two crystalline phases, and these are the cubic and rhombohedral (corundum) structures.[50] Based on this, it fits well that the iridium deposition in this work results in predominantly metallic iridium species, as Ir(0) is mostly found in the face-centered-cubic phase;[51] therefore, this oxidation state of iridium could have been preferred over the rutile phase to minimize the surface free energy of ITO-supported catalysts during the deposition process. CAT-C, which utilizes ITO support with 10% Sn dopant shows the highest concentration of Sn species at the surface (see Table S3 in the Supporting Information). Such conditions could have potentially influenced the

https://doi.org/10.1021/acs.jpcc.2c06501
J. Phys. Chem. C 2023, 127, 894–906

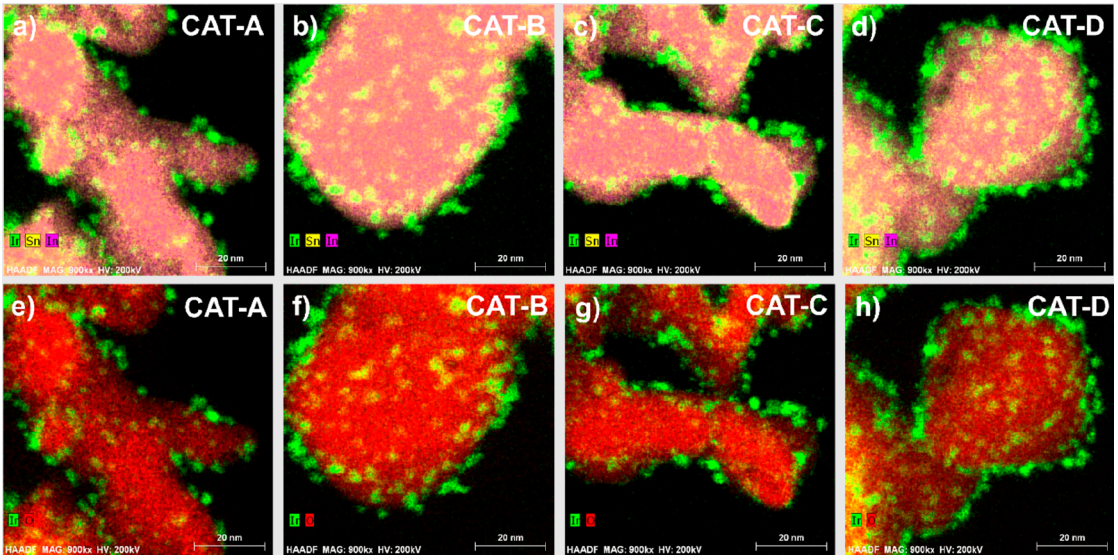

Figure 4. HR-STEM EDX color composite maps for CAT-A to CAT-D. (a–d) display overlaps among Ir (green), Sn (yellow), and In (magenta), while (e–h) illustrate overlap between Ir (green) and O (red).

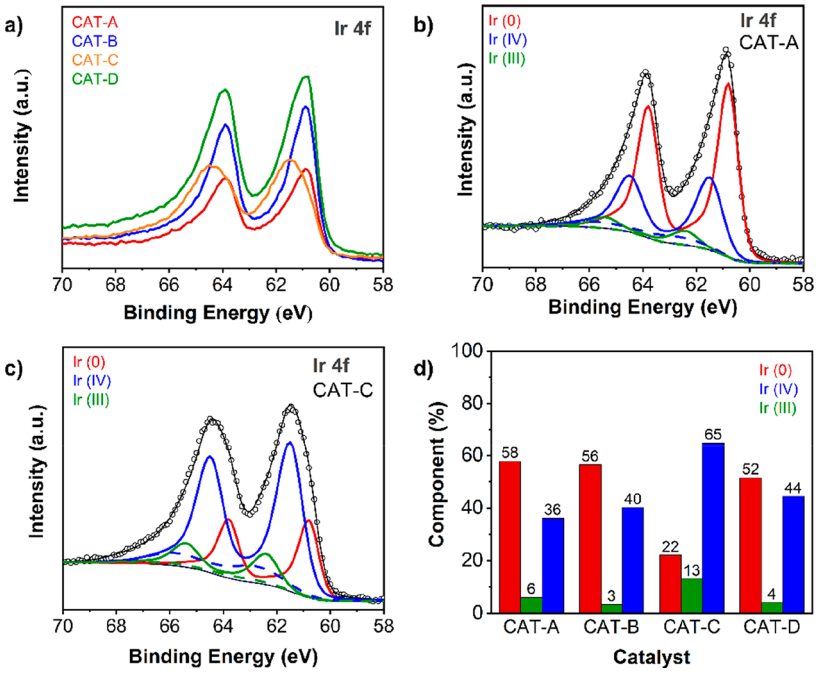

Figure 5. Ir 4f XPS spectra, where (a) displays the high resolution Ir 4f XPS spectra measured from all catalysts, (b) and (c) show the curve-fitting of Ir 4f for CAT-A and CAT-C, respectively, where Ir(0) (red line), Ir(IV) (blue line), Ir(III) (green line), Ir(IV) satellites (blue dashed lines), and Ir(III) satellites (green dashed line) are shown, and (d) is the Ir component contributions.

preferential formation of Ir(IV) species.[41] Considering identical conditions were applied for both ATO and ITO deposition processes, our results strongly suggest that the support material can significantly affect the nature of the Ir species forming during the MOCD process.

The same In and Sn surface species as found in ITO supports were measured from all catalysts (postdeposition), and their component ratios are summarized in Table 4. Regarding the O 1s spectra (see Figure S5 in the Supporting Information), although the oxygen components identified are similar to those observed on the ITO support (predeposition), there is a shift in the quantities present, particularly with the oxygen bonded to hydrocarbon species, which could be due to incomplete removal of the $Ir(acac)_3$.[27] This is further supported by examples of C 1s spectra (see Figure S4 in the Supporting Information), where a higher contribution is obtained from carbon species bonded to oxygen in the energy range 286.0–290.0 eV for the supported catalysts compared to results for the bare ITO supports.

Chemical Stability of the Support and Deposited Catalyst. To understand the influence of the chemical stability of the support on the electrochemical stability of the catalysts, the ITO supports (ITO-A and ITO-B), and their corresponding MOCD IrO_x/ITO catalysts, CAT-A and CAT-B were evaluated by a time-based chemical dissolution in the 0.1 M $HClO_4$ electrolyte. ICP-OES measurements were performed

https://doi.org/10.1021/acs.jpcc.2c06501
J. Phys. Chem. C 2023, 127, 894–906

Table 4. Summary of Key Results of the MOCD IrO_x/ITO Catalysts, with Comparison to a IrO_2−TiO_2 Commercial Benchmark and the MOCD IrO_2/ATO Catalyst

	surface component ratio (XPS)				electrochemical performance				
sample id	Sn(II) /Sn(IV)	$In(OH_3)$ /In_2O_3	Ir(IV) /Ir(III)	Ir(0) /Ir(III)	initial mass-specific OER activity (A g_{Ir}^{-1})	after 1.60 V CA mass-specific OER activity (A g_{Ir}^{-1})	relative OER activity loss (%)	initial Tafel slope value (mV dec^{-1})	after 1.60 V CA Tafel slope value (mV dec^{-1})
CAT-A	2	0.4	6	10	299 ± 29	27 ± 23	91	54 ± 4	84 ± 4
CAT-B	5	0.3	13	19	207 ± 34	195 ± 40	6	57 ± 7	49 ± 2
CAT-C	2	0.2	5	2	119 ± 10	68 ± 10	43	62 ± 6	70 ± 4
CAT-D	5	0.2	11	13	156 ± 15	116 ± 23	26	58 ± 1	52 ± 2
MOCD IrO_2/ATO			3	0.2	72	47	35	63 ± 4	58 ± 1
IrO_2-TiO_2commercial benchmark					11.9 ± 3.3	3.6 ± 1.8	70	54 ± 2	61 ± 1
Ir black commercial benchmark					44 ± 1.0	41 ± 1.3	7	53 ± 2.0	44 ± 1.6

on the supernatant to quantify the dissolved species. Figure 6 shows the chemical dissolution profiles over a period of 24 h, while Table S4 in the Supporting Information summarizes the calculated dissolution percentages for the support and the supported catalysts.

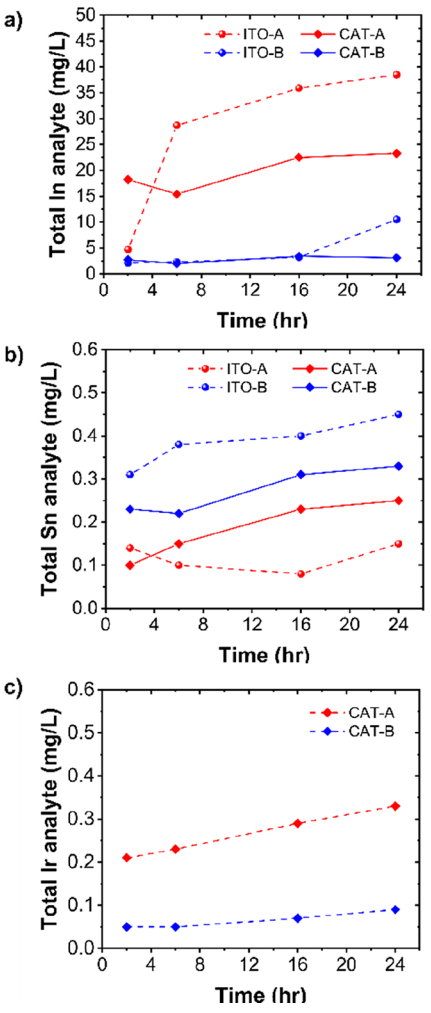

Figure 6. Chemical dissolution profiles of ITO-A, ITO-B, CAT-A, and CAT-B: (a) total In analyte concentration, (b) total Sn analyte concentration, and (c) total Ir analyte concentration present in the supernatant of the samples after 24 h, respectively.

It was seen that CAT-A is more chemically unstable than CAT-B as CAT-A suffers from a greater loss of In (∼65%) from the ITO support than CAT-B (∼9%) after 24 h. This is consistent with the results for ITO-A compared to those for ITO-B, where a rapid increase in In concentration in the supernatant solution is observed for ITO-A (∼93%) compared to only ∼25% for ITO-B. CAT-A and CAT-B in comparison to ITO-A and ITO-B have smaller amounts of dissolved In concentrations present overall after 24 h of the stability test. CAT-A displays a significantly larger amount of dissolved Ir (∼92%) than CAT-B (∼18%) after 24 h of the stability test.

The higher chemical stability observed from the low-SSA ITO support (ITO-B) was found to further increase in the case of the corresponding catalyst (CAT-B). Furthermore, it was observed that the chemical stability improved for both ITO supports after the deposition of the IrO_x nanoparticles. This suggests that the presence of the IrO_x nanoparticles possibly had a stabilizing effect on the ITO support.

Electrochemical Oxygen Evolution Reaction Performance. The initial OER performance reported in terms of Ir mass-specific activity at 1.525 V vs RHE indicated that CAT-A and CAT-B are the most promising as they have significantly higher mass-specific OER activities compared to those of CAT-C and CAT-D (refer to Figure 7a). These activities were 10−25 times better than that of the IrO_2−TiO_2 commercial benchmark, 4−7 times larger compared to that of the Ir Black commercial benchmark, and 2−4 times greater than that of the MOCD IrO_2/ATO catalyst tested under the same conditions.[27]

The difference in stabilities of CAT-A and CAT-B is showcased in the Tafel slopes. Figure 7b illustrates the Tafel slopes for CAT-A and CAT-B of 54 and 57 mV dec^{-1}, which changed after the stability testing to 84 and 49 mV dec^{-1}, respectively. The degradation of CAT-A, CAT-B, and the IrO_2−TiO_2 commercial benchmark is further illustrated by Figure S7 in the Supporting Information, where the current response during the 2 h stability hold was plotted. Initial Tafel slopes were comparable to values reported for unsupported iridium oxides (50−60 mV dec^{-1}) as well as for the IrO_2−TiO_2 benchmark (54 mV dec^{-1}) previously reported.[19,27,52] The increase in the Tafel slope value for CAT-A after the stability test is most likely correlated to the higher degree of In and Ir dissolution, as evidenced from the chemical stability tests, that may result in a loss of electrical conductivity during the OER performance evaluation. Similar effects were also previously reported with low catalyst loadings on ATO.[27] The

https://doi.org/10.1021/acs.jpcc.2c06501
J. Phys. Chem. C 2023, 127, 894−906

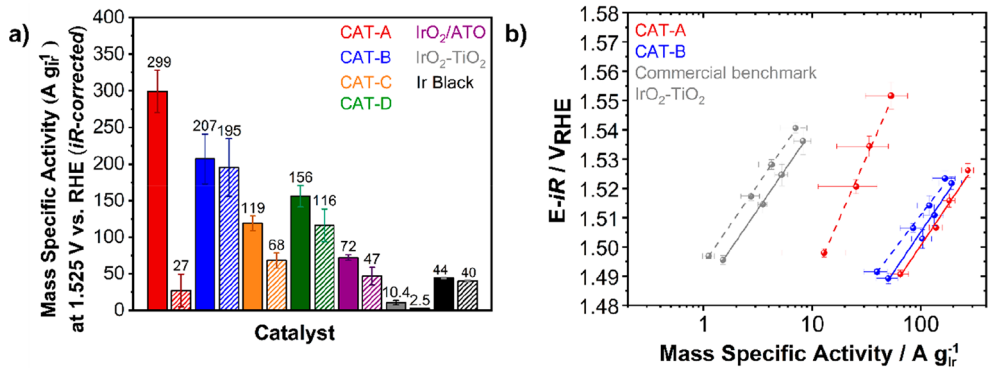

Figure 7. (a) *Ex-situ* mass-specific OER activities of the prepared IrO_x/ITO catalysts, the IrO_2−TiO_2 and Ir black commercial catalysts, and the previously published MOCD IrO_2/ATO catalyst before (solid bar) and after (pattern bar) stability testing by chronoamperometry. (b) Mass-specific Tafel slopes for CAT-A and CAT-B, before (solid line) and after (dashed line) stability testing by chronoamperometry.

slight drop in the Tafel slope value for CAT-B is most likely correlated to the degree of hydration of the hydrous, amorphous IrO_x that formed electrochemically during the OER performance evaluation.[53]

To understand the influence of the physicochemical properties of ITO supports on the initial OER activities of the prepared catalysts, several catalyst−support correlations need to be taken into consideration. These include the average IrO_x particle size and interparticle distance, Ir metal loading, Ir phase, and support dopant ratio. However, from thorough physical characterization and electrochemical analysis of the prepared catalysts, it can be concluded that both particle size effects and Ir loading effects are not responsible for the differences in catalyst activities for the various ITO-supported catalysts, as the use of MOCD resulted in virtually identical IrO_x particles sizes and similar iridium loadings across all the synthesized materials. Therefore, the main difference in the performance of these catalysts can be attributed to other influences, such as particle proximity and coverage effects. It is therefore possible to distinguish the prepared catalysts materials based on their interparticle distances, which vary with support SSAs. A similar approach was previously reported for Pt/C catalysts where the Pt loading was varied on the same supports.[35,49,54] However, in the case of the present work, the SSA of the supports was varied while keeping the Ir loading and particle size practically equivalent. Therefore, for high-SSA supports (CAT-A and -C), the interparticle distance is approximately 4 times larger than for low-SSA supports (CAT-B and -D) (see Table S2). However, as with previous studies, a significant degree of IrO_x agglomeration was observed on low-SSA supports (Figure 3b,d).

Furthermore, from XPS analysis, it can be concluded that the surface composition of the ITO support influences the nature of the deposited IrO_x nanoparticles. Figure 8a,b illustrates correlations found between electrocatalyst surface ratio components and the ITO average BET surface area. It is clear from Figure 8a that in catalysts utilizing low-SSA supports, higher surface Sn(II)/Sn(IV) component ratios were observed. Figure 8b shows that for catalysts formed on lower average SSA supports, higher surface Ir(IV)/Ir(III) component ratios were measured from the deposited IrO_x nanoparticles. This indicates that Sn species enriched on the ITO surface have potentially influenced the preferential formation of Ir(IV).

Therefore, for comparison of catalysts with the same support SSA, the differences in performance between CAT-A and

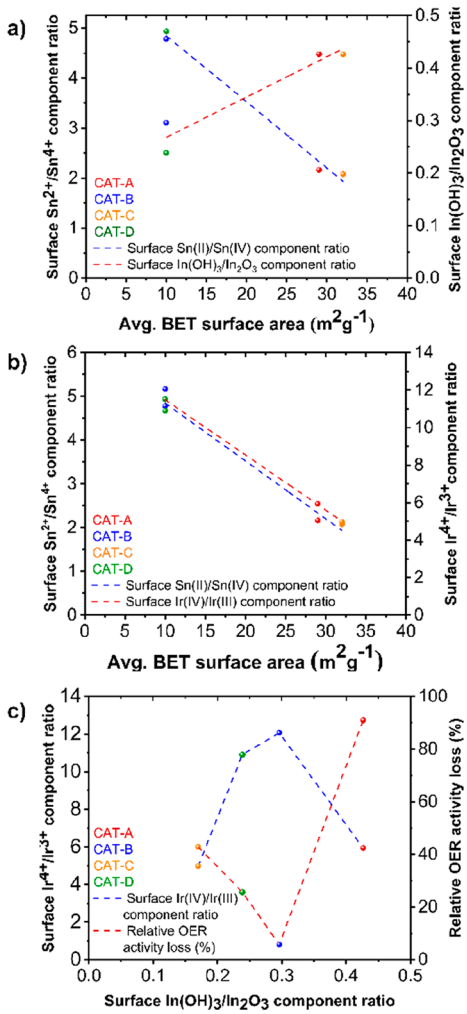

Figure 8. Correlations between the catalysts' surface components: (a) Sn and In surface components vs average BET surface area, (b) Sn and Ir surface components vs average BET surface area, and (c) In and Ir surface components vs relative OER activity loss.

CAT-C are accounted for by the nature of the Ir phase present, where CAT-A has a greater amount of Ir(0) species present and a higher initial OER activity. This also accounts for the relatively high initial OER activities for CAT-B and -D. In these catalysts, Ir(0) was the dominant species (Figure 5d), which contributed to their initial large mass-specific activity in

https://doi.org/10.1021/acs.jpcc.2c06501
J. Phys. Chem. C 2023, 127, 894−906

comparison to results for CAT-C. Coincidently, this also accounts for the activity of the ITO-supported IrO_x catalysts exhibiting higher initial OER activities than the ATO-supported IrO_2 catalyst prepared under the same conditions; this can be explained by the presence of highly active, amorphous electrochemically generated iridium oxides, which are formed by the Ir(0) species that dominate on the surface of MOCD IrO_2/ITO in comparison to the rutile IrO_2 species reported by Rajan et al.[27] for MOCD IrO_2/ATO.[29,42,52,55,56] However, in the case of CAT-B and -D, the lower OER activities in comparison to those of CAT-A could be explained by the higher degree of agglomeration, shorter interparticle distances, and thereby reduced Ir utilization.

However, as Ir(III) is most likely to undergo iridium dissolution, the presence of this species formed electrochemically could contribute significantly to the instability of the catalysts. The catalysts with low-SSA supports exhibited higher stability via chronoamperometry analysis compared to those on higher SSA supports, with CAT-B experiencing only a 6% relative loss of oxygen evolution mass activity (see Table 4). The most active catalyst, CAT-A, is the least stable MOCD IrO_x/ITO electrocatalyst, while in comparison, the IrO_2−TiO_2 commercial benchmark demonstrated a 70% activity loss. CAT-B and CAT-D, both made from low-SSA supports, have similar Ir, Ir(IV), and Ir(III) amounts, but the initial activity of CAT-B is greater, and the catalyst is more stable. Given the similarity in IrO_x particle size, loading, and phase, we can only attribute this small difference in activity to differences in support conductivity given by their different dopant ratios. In addition, lower $In(OH)_3/In_2O_3$ ratios were also observed from XPS analysis. Figure 8c shows that CAT-B has a lower surface $In(OH)_3/In_2O_3$ ratio and a greater surface Ir(IV)/Ir(III) component ratio than CAT-A, which has an influence on the electrochemical stability of this catalyst (Table 4). CAT-B was seen to have the highest Ir(0)/Ir(III) component ratio value (Table 4). It is speculated that the higher $In(OH)_3/In_2O_3$ ratio measured from catalysts (postdeposition) would contribute to their lower stability due to dissolution of the $In(OH)_3$ species. The possible stabilization of the ITO support by the deposited catalyst particles with a higher degree of coverage is supported by the chemical stability tests (Figure 6). Higher coverage of IrO_x nanoparticles and lower interparticle distances on low-SSA ITO supports resulted in more electrochemically stable catalysts. In those catalysts, the ITO surface is less exposed, as it is protected by the deposited IrO_x nanoparticles, which makes it less susceptible to chemical degradation.

It is also evident that CAT-A and -B, which utilize lower dopant concentration ITO supports (Table 1) demonstrated higher activities compared to those made on higher dopant concentration ITO. However, these catalysts also differ in terms of BET SSA and surface nature: Sn(II)/Sn(IV) and Ir(IV)/Ir(III) component ratios, which would further complicate attempts to discuss the possible effect of the Sb dopant concentration on the catalyst performance. To understand the influence of the support's dopant concentration on the overall catalyst activity, it is necessary to first summarize an important conclusion regarding OER activities for IrO_x/ITO catalysts reported in the literature. The highest performing catalysts reported were that of IrO_x layers[34] and atomically dispersed[30] Ir atoms supported on ITO supports. In these studies, Ir utilization was maximized by availing the highest fraction of surface sites for OER electrocatalysis. However, considering IrO_x particles in the size range 1−5 nm (Figure 9),

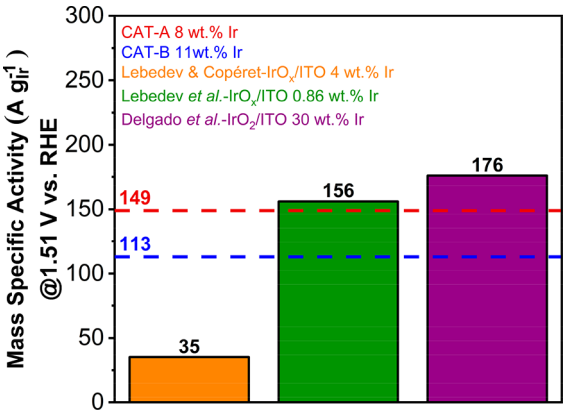

Figure 9. Average mass-specific OER activities of IrO_x/ITO catalysts reported in recent literature compared to those of CAT-A and CAT-B, indicated by red and blue lines, respectively.

as is also the case with the catalysts prepared in this study, it is seen that reported literature data confirm that there is a clear Ir loading dependence on the initial OER performance. Delgado et al.[28] reported the highest OER activity of 176 A g_{Ir}^{-1} at 1.51 V vs RHE at 30 wt % Ir supported on ITO. Interestingly, the mass activity of IrO_x supported on undoped SnO_2 was only 6% lower in the same study. A similar effect was observed by Geiger et al.,[33] where differences in the performance of ITO-supported IrO_x catalysts compared to SnO_2-supported IrO_x catalysts at loadings of 20 wt % can be accounted for by differences in the IrO_x particle size at these loadings. In contrast, at significantly lower Ir loadings of 4 wt %, Lebedev and Coperet[29] reported a considerably lower activity of 35 A g_{Ir}^{-1} at 1.51 vs RHE. Therefore, it can be concluded that the Ir loading is a significant factor determining the catalyst activity.

In this work, CAT-B and CAT-D have identical Ir loadings, identical SSAs, similar nanoparticle coverages, and similar natures in terms of surface Sn(II)/Sn(IV) and Ir(IV)/Ir(III) component ratios. The only difference is the ITO support Sn dopant concentration (5% for CAT-B and 10% for CAT-D). Therefore, these two catalysts are the most suitable to evaluate the possible effect of the ITO dopant level on catalyst performance. These catalysts demonstrate only a 25% difference in their activities, which suggests that at sufficiently high Ir loadings, the effect of support conductivity is minimized.

Here it is postulated that at high Ir wt % loadings, or in cases where higher Ir coverages are present, i.e., low interparticle distances, the need for a conductive support becomes less crucial, particularly when particle agglomeration is observed. This can be explained by enhanced electrical percolation in catalysts with greater particle coverage, as the closely located nanoparticles of IrO_x could potentially form an electronically conductive network across the support, facilitating the OER and to some extent, minimizing the need for a conductive support material. However, to further improve the performance of supported catalysts for the OER, a drive toward lower iridium loadings is still needed. For supported IrO_x catalysts with low Ir metal loadings, there appears to still be a need for a highly conductive support material that is both chemically and electrochemically stable. From these results, an ITO-supported electrocatalyst, CAT-B, with low iridium loading of 11 wt %, proved to be more active and relatively more stable than the commercial benchmark (with a significantly higher iridium

https://doi.org/10.1021/acs.jpcc.2c06501
J. Phys. Chem. C 2023, 127, 894−906

loading of 75 wt %) and to MOCD IrO_2/ATO catalyst. As such, the MOCD method for deposition of iridium-based catalysts on oxide supports has been successfully extended to ITO support materials, where the prepared catalysts demonstrated promising electrochemical performance in relation to both published IrO_x/ATO and IrO_x/ITO prepared catalysts. This could be a consequence of greater iridium utilization, as well as the effect of the iridium phase present over a more conductive support, indicating a potential interplay among the IrO_x phase, the particle size, and the interparticle distance on OER performance.

4. CONCLUSIONS

In summary, this study demonstrated the versatility of the MOCD method for the preparation of well-controlled, evenly distributed, small IrO_x nanoparticles of ~2 nm with equivalent Ir metal loadings across the surface of tin-doped indium oxide (ITO) support materials. By varying the specific surface area (SSA) of the support and dopant weight ratios (Sn:In), it was possible to study the effect of various physicochemical properties of the support on the nature of the deposited IrO_x nanoparticle phase and their influence on OER performance. The nature of the ITO support surface was found to influence the Ir phase present and coverage of the deposited IrO_x nanoparticles, with the latter related to the interparticle distance. IrO_x/ITO catalysts prepared on low specific surface area ITO supports had higher surface Sn(II)/Sn(IV) and Ir(IV)/Ir(III) component ratios than those prepared on the high-SSA ITO supports. The nature of the IrO_x (x = 0−2) nanoparticles influenced the electrochemical activity of the electrocatalysts as metallic iridium was found to be the predominant Ir component. Furthermore, the larger interparticle distance as a result of lower coverages on high-SSA supports was found to significantly increase the initial OER activity, by maximizing Ir utilization at the expense of electrochemical stability under OER conditions. By comparing the activities of catalysts with the same surface composition, SSA, and interparticle distance across varying dopant ratios, we found that there is possible a trade-off between Ir loadings on the effect of electrical conductivity of the support, where at higher loadings support conductivity effects are possibly minimized. Overall, the high-performing and most durable catalyst was found to be the product of the interplay between the Ir phases present with low interparticle distances, where the material is stabilized by the higher extent of IrO_x coverage over the support. These findings highlight the importance of decoupling of several physicochemical support catalyst−support relations and their subsequent influence on OER performance. However, considering these results were obtained *ex situ* using an RDE set up, further testing is currently underway to correlate these results with *in-situ* electrolyzer performance.

■ ASSOCIATED CONTENT

Supporting Information

The Supporting Information is available free of charge at https://pubs.acs.org/doi/10.1021/acs.jpcc.2c06501.

Additional physicochemical characterization data (XRD graphs, HR-STEM data, lattice spacings and particle sizes, XPS spectra and component contributions, and chemical dissolution quantitative data) and electrochemical characterization data (absolute current vs time graph) of the samples (PDF)

■ AUTHOR INFORMATION

Corresponding Author

Rhiyaad Mohamed − *HySA/Catalysis Centre of Competence, Catalysis Institute, Department of Chemical Engineering, University of Cape Town, Cape Town 7701, South Africa;* orcid.org/0000-0002-3857-1162; Email: rhiyaad.mohamed@uct.ac.za

Authors

Julie-Ann Hoffman − *HySA/Catalysis Centre of Competence, Catalysis Institute, Department of Chemical Engineering, University of Cape Town, Cape Town 7701, South Africa; Department of Chemistry, Cape Peninsula University of Technology, Cape Town 8000, South Africa*

Ziba S. H. S. Rajan − *HySA/Catalysis Centre of Competence, Catalysis Institute, Department of Chemical Engineering, University of Cape Town, Cape Town 7701, South Africa;* orcid.org/0000-0002-1148-9601

Darija Susac − *HySA/Catalysis Centre of Competence, Catalysis Institute, Department of Chemical Engineering, University of Cape Town, Cape Town 7701, South Africa*

Mangaka C. Matoetoe − *Department of Chemistry, Cape Peninsula University of Technology, Cape Town 8000, South Africa*

Complete contact information is available at: https://pubs.acs.org/10.1021/acs.jpcc.2c06501

Notes

The authors declare no competing financial interest.

■ ACKNOWLEDGMENTS

We thank the South African Department of Science and Innovation for the financial support in the form of HySA/Catalysis Centre of Competence programme funding. For the electron microscopy unit at the University of Cape Town, in particular, Ms N. Hanief is acknowledged for her assistance with SEM-EDX and TEM measurements. We thank Prof. Patricia Kooyman for her contribution in TEM characterisation. We acknowledge the 4D laboratories at Simon Fraser University (Canada), Dr. Michael Wang for XPS measurements, and Dr. Lis Guimaraes de Azeredo Melo for generating HR-STEM EDX maps.

■ REFERENCES

(1) Shirvanian, P.; van Berkel, F. Novel components in Proton Exchange Membrane (PEM) Water Electrolyzers (PEMWE): Status, challenges and future needs. A mini review. *Electrochem. Commun.* **2020**, *114*, 106704.

(2) Stiber, S.; Sata, N.; Morawietz, T.; Ansar, S. A.; Jahnke, T.; Lee, J. K.; Bazylak, A.; Fallisch, A.; Gago, A. S.; Friedrich, K. A. A high-performance, durable and low-cost proton exchange membrane electrolyser with stainless steel components. *Energy Environ. Sci.* **2022**, *15* (1), 109−122.

(3) Ahmad Kamaroddin, M. F.; Sabli, N.; Tuan Abdullah, T. A.; Siajam, S. I.; Abdullah, L. C.; Abdul Jalil, A.; Ahmad, A. Membrane-Based Electrolysis for Hydrogen Production: A Review. *Membranes (Basel)* **2021**, *11* (11), 810.

(4) Shiva Kumar, S.; Himabindu, V. Hydrogen production by PEM water electrolysis − A review. *Materials Science for Energy Technologies* **2019**, *2* (3), 442−454.

(5) Fabbri, E.; Habereder, A.; Waltar, K.; Kotz, R.; Schmidt, T. J. Developments and perspectives of oxide-based catalysts for the oxygen evolution reaction. *Catalysis Science & Technology* **2014**, *4* (11), 3800−3821.
(6) Carmo, M.; Fritz, D. L.; Merge, J.; Stolten, D. A comprehensive review on PEM water electrolysis. *Int. J. Hydrogen Energy* **2013**, *38* (12), 4901−4934.
(7) Chatenet, M.; Pollet, B. G.; Dekel, D. R.; Dionigi, F.; Deseure, J.; Millet, P.; Braatz, R. D.; Bazant, M. Z.; Eikerling, M.; Staffell, I.; et al. Water electrolysis: from textbook knowledge to the latest scientific strategies and industrial developments. *Chem. Soc. Rev.* **2022**, *51* (11), 4583−4762.
(8) Reier, T.; Nong, H. N.; Teschner, D.; Schlogl, R.; Strasser, P. Electrocatalytic Oxygen Evolution Reaction in Acidic Environments - Reaction Mechanisms and Catalysts. *Adv. Energy Mater.* **2017**, *7* (1), 1601275.
(9) Qu, H. Y.; He, X. W.; Wang, Y. B.; Hou, S. Electrocatalysis for the Oxygen Evolution Reaction in Acidic Media: Progress and Challenges. *Applied Sciences-Basel* **2021**, *11* (10), 4320.
(10) Abbott, D. F.; Lebedev, D.; Waltar, K.; Povia, M.; Nachtegaal, M.; Fabbri, E.; Copere, C.; Schmidt, T. J. Iridium Oxide for the Oxygen Evolution Reaction: Correlation between Particle Size, Morphology, and the Surface Hydroxo Layer from Operando XAS. *Chem. Mater.* **2016**, *28* (18), 6591−6604.
(11) Marshall, A.; Borresen, B.; Hagen, G.; Sunde, S.; Tsypkin, M.; Tunold, R. Iridium oxide-based nanocrystalline particles as oxygen evolution electrocatalysts. *Russian Journal of Electrochemistry* **2006**, *42* (10), 1134−1140.
(12) Massue, C.; Pfeifer, V.; Huang, X.; Noack, J.; Tarasov, A.; Cap, S.; Schlogl, R. High-Performance Supported Iridium Oxohydroxide Water Oxidation Electrocatalysts. *ChemSusChem* **2017**, *10* (9), 1943−1957.
(13) Trasatti, S. Electrocatalysis in the Anodic Evolution of Oxygen and Chlorine. *Electrochim. Acta* **1984**, *29* (11), 1503−1512.
(14) Wei, C.; Rao, R. R.; Peng, J.; Huang, B.; Stephens, I. E. L.; Risch, M.; Xu, Z. J.; Shao-Horn, Y. Recommended Practices and Benchmark Activity for Hydrogen and Oxygen Electrocatalysis in Water Splitting and Fuel Cells. *Adv. Mater.* **2019**, *31* (31), e1806296.
(15) Minke, C.; Suermann, M.; Bensmann, B.; Hanke-Rauschenbach, R. Is iridium demand a potential bottleneck in the realization of large-scale PEM water electrolysis? *Int. J. Hydrogen Energy* **2021**, *46* (46), 23581−23590.
(16) Pushkarev, A. S.; Pushkareva, I. V.; Bessarabov, D. G. Supported Ir-Based Oxygen Evolution Catalysts for Polymer Electrolyte Membrane Water Electrolysis: A Minireview. *Energy Fuels* **2022**, *36* (13), 6613−6625.
(17) Puthiyapura, V. K.; Pasupathi, S.; Su, H. N.; Liu, X. T.; Pollet, B.; Scott, K. Investigation of supported IrO2 as electrocatalyst for the oxygen evolution reaction in proton exchange membrane water electrolyser. *Int. J. Hydrogen Energy* **2014**, *39* (5), 1905−1913.
(18) Hartig-Weiss, A.; Miller, M.; Beyer, H.; Schmitt, A.; Siebel, A.; Freiberg, A. T. S.; Gasteiger, H. A.; El-Sayed, H. A. Iridium Oxide Catalyst Supported on Antimony-Doped Tin Oxide for High Oxygen Evolution Reaction Activity in Acidic Media. *Acs Applied Nano Materials* **2020**, *3* (3), 2185−2196.
(19) Oh, H. S.; Nong, H. N.; Reier, T.; Bergmann, A.; Gliech, M.; Ferreira de Araujo, J.; Willinger, E.; Schlogl, R.; Teschner, D.; Strasser, P. Electrochemical Catalyst-Support Effects and Their Stabilizing Role for IrOx Nanoparticle Catalysts during the Oxygen Evolution Reaction. *J. Am. Chem. Soc.* **2016**, *138* (38), 12552−12563.
(20) Xu, J. Y.; Liu, G. Y.; Li, J. L.; Wang, X. D. The electrocatalytic properties of an IrO2/SnO2 catalyst using SnO2 as a support and an assisting reagent for the oxygen evolution reaction. *Electrochim. Acta* **2012**, *59*, 105−112.
(21) Sapountzi, F. M.; Gracia, J. M.; Weststrate, C. J.; Fredriksson, H. O. A.; Niemantsverdriet, J. W. Electrocatalysts for the generation of hydrogen, oxygen and synthesis gas. *Prog. Energy Combust. Sci.* **2017**, *58*, 1−35.
(22) Sasaki, K.; Hayashi, S.; Kanda, K.; Takabatake, Y.; Tsukatsune, T.; Higashi, T.; Takasaki, F.; Noda, Z.; Hayashi, A. Alternative Electrocatalyst Support Materials for Polymer Electrolyte Fuel Cells. *ECS Meeting Abstracts* **2012**, *MA2012-02* (13), 1684−1684.
(23) Böhm, D.; Beetz, M.; Schuster, M.; Peters, K.; Hufnagel, A. G.; Döblinger, M.; Böller, B.; Bein, T.; Fattakhova-Rohlfing, D. Efficient OER Catalyst with Low Ir Volume Density Obtained by Homogeneous Deposition of Iridium Oxide Nanoparticles on Macroporous Antimony-Doped Tin Oxide Support. *Adv. Funct. Mater.* **2020**, *30* (1), 1906670.
(24) Oh, H. S.; Nong, H. N.; Strasser, P. Preparation of Mesoporous Sb-, F-, and In-Doped SnO2 Bulk Powder with High Surface Area for Use as Catalyst Supports in Electrolytic Cells. *Adv. Funct. Mater.* **2015**, *25* (7), 1074−1081.
(25) Puthiyapura, V. K.; Mamlouk, M.; Pasupathi, S.; Pollet, B. G.; Scott, K. Physical and electrochemical evaluation of ATO supported IrO2 catalyst for proton exchange membrane water electrolyser. *J. Power Sources* **2014**, *269*, 451−460.
(26) Solà-Hernández, L.; Claudel, F.; Maillard, F.; Beauger, C. Doped tin oxide aerogels as oxygen evolution reaction catalyst supports. *Int. J. Hydrogen Energy* **2019**, *44* (45), 24331−24341.
(27) Rajan, Z. S. H. S.; Binninger, T.; Kooyman, P. J.; Susac, D.; Mohamed, R. Organometallic chemical deposition of crystalline iridium oxide nanoparticles on antimony-doped tin oxide support with high-performance for the oxygen evolution reaction. *Catalysis Science & Technology* **2020**, *10* (12), 3938−3948.
(28) Delgado, S.; Lakhtaria, P.; Sousa, E.; Lagarteira, T.; Friedrich, K. A.; Mendes, A. Towards stable and highly active IrO2 catalysts supported on doped tin oxides for the oxygen evolution reaction in acidic media. *E3S Web Conf.* **2022**, *334*, 03001.
(29) Lebedev, D.; Coperet, C. Small, Narrowly Distributed Iridium Nanoparticles Supported on Indium Tin Oxide for Efficient Anodic Water Oxidation. *Acs Applied Energy Materials* **2019**, *2* (1), 196−200.
(30) Lebedev, D.; Ezhov, R.; Heras-Domingo, J.; Comas-Vives, A.; Kaeffer, N.; Willinger, M.; Solans-Monfort, X.; Huang, X.; Pushkar, Y.; Coperet, C. Atomically Dispersed Iridium on Indium Tin Oxide Efficiently Catalyzes Water Oxidation. *ACS Cent Sci.* **2020**, *6* (7), 1189−1198.
(31) da Silva, G. C.; Venturini, S. I.; Zhang, S.; Löffler, M.; Scheu, C.; Mayrhofer, K. J. J.; Ticianelli, E. A.; Cherevko, S. Oxygen Evolution Reaction on Tin Oxides Supported Iridium Catalysts: Do We Need Dopants? *ChemElectroChem.* **2020**, *7* (10), 2330−2339.
(32) Benck, J. D.; Pinaud, B. A.; Gorlin, Y.; Jaramillo, T. F. Substrate selection for fundamental studies of electrocatalysts and photoelectrodes: inert potential windows in acidic, neutral, and basic electrolyte. *PLoS One* **2014**, *9* (10), e107942.
(33) Geiger, S.; Kasian, O.; Mingers, A. M.; Mayrhofer, K. J. J.; Cherevko, S. Stability limits of tin-based electrocatalyst supports. *Sci. Rep* **2017**, *7* (1), 4595.
(34) Ledendecker, M.; Geiger, S.; Hengge, K.; Lim, J.; Cherevko, S.; Mingers, A. M.; Gohl, D.; Fortunato, G. V.; Jalalpoor, D.; Schuth, F.; et al. Towards maximized utilization of iridium for the acidic oxygen evolution reaction. *Nano Research* **2019**, *12* (9), 2275−2280.
(35) Taylor, S.; Fabbri, E.; Levecque, P.; Schmidt, T. J.; Conrad, O. The Effect of Platinum Loading and Surface Morphology on Oxygen Reduction Activity. *Electrocatalysis* **2016**, *7* (4), 287−296.
(36) Jackson, C.; Conrad, O.; Levecque, P. Systematic Study of Pt-Ru/C Catalysts Prepared by Chemical Deposition for Direct Methanol Fuel Cells. *Electrocatalysis* **2017**, *8* (3), 224−234.
(37) Mohamed, R.; Binninger, T.; Kooyman, P. J.; Hoell, A.; Fabbri, E.; Patru, A.; Heinritz, A.; Schmidt, T. J.; Levecque, P. Facile deposition of Pt nanoparticles on Sb-doped SnO2 support with outstanding active surface area for the oxygen reduction reaction. *Catalysis Science & Technology* **2018**, *8* (10), 2672−2685.
(38) Jackson, C.; Smith, G. T.; Mpofu, N.; Dawson, J. M. S.; Khoza, T.; September, C.; Taylor, S. M.; Inwood, D. W.; Leach, A. S.; Kramer, D.; et al. A quick and versatile one step metal-organic chemical deposition method for supported Pt and Pt-alloy catalysts. *RSC Adv.* **2020**, *10* (34), 19982−19996.

https://doi.org/10.1021/acs.jpcc.2c06501
J. Phys. Chem. C 2023, 127, 894−906

(39) Detweiler, Z. M.; Wulfsberg, S. M.; Frith, M. G.; Bocarsly, A. B.; Bernasek, S. L. The oxidation and surface speciation of indium and indium oxides exposed to atmospheric oxidants. *Surf. Sci.* **2016**, *648*, 188−195.
(40) Donley, C.; Dunphy, D.; Paine, D.; Carter, C.; Nebesny, K.; Lee, P.; Alloway, D.; Armstrong, N. R. Characterization of Indium−Tin Oxide Interfaces Using X-ray Photoelectron Spectroscopy and Redox Processes of a Chemisorbed Probe Molecule: Effect of Surface Pretreatment Conditions. *Langmuir* **2002**, *18* (2), 450−457.
(41) Teterin, Y. A.; Maslakov, K. I.; Murav'ev, E. N.; Teterin, A. Y.; Bulychev, N. A.; Meshkov, B. B.; Stepnov, D. S. X-ray Photoelectron Spectroscopy Study of Indium Tin Mixed Oxides on the Surface of Silicate Glass. *Inorg. Mater.* **2020**, *56* (5), 482−493.
(42) Pfeifer, V.; Jones, T. E.; Velasco Velez, J. J.; Massue, C.; Greiner, M. T.; Arrigo, R.; Teschner, D.; Girgsdies, F.; Scherzer, M.; Allan, J.; et al. The electronic structure of iridium oxide electrodes active in water splitting. *Phys. Chem. Chem. Phys.* **2016**, *18* (4), 2292−2296.
(43) Yu, H. R.; Danilovic, N.; Wang, Y.; Willis, W.; Poozhikunnath, A.; Bonville, L.; Capuano, C.; Ayers, K.; Maric, R. Nano-size IrOx catalyst of high activity and stability in PEM water electrolyzer with ultra-low iridium loading. *Appl. Catal., B* **2018**, *239*, 133−146.
(44) Schmidt, T. J.; Gasteiger, H. A.; Stäb, G. D.; Urban, P. M.; Kolb, D. M.; Behm, R. J. Characterization of High-Surface-Area Electrocatalysts Using a Rotating Disk Electrode Configuration. *J. Electrochem. Soc.* **1998**, *145* (7), 2354−2358.
(45) Garcia, A. C.; Koper, M. T. M. Effect of Saturating the Electrolyte with Oxygen on the Activity for the Oxygen Evolution Reaction. *ACS Catal.* **2018**, *8* (10), 9359−9363.
(46) Oakton, E.; Lebedev, D.; Povia, M.; Abbott, D. F.; Fabbri, E.; Fedorov, A.; Nachtegaal, M.; Copéret, C.; Schmidt, T. J. IrO2-TiO2: A High-Surface-Area, Active, and Stable Electrocatalyst for the Oxygen Evolution Reaction. *ACS Catal.* **2017**, *7* (4), 2346−2352.
(47) Biesinger, M. C. https://www.xpsfitting.com/ (accessed 09 September 2022).
(48) Naumkin, A. V.; K.-V, A.; Gaarenstroom, S. W.; Powell, C. J. *NIST X-ray Photoelectron Spectroscopy Database*. https://srdata.nist.gov/xps/Default.aspx (accessed 09 September 2022).
(49) Inaba, M.; Zana, A.; Quinson, J.; Bizzotto, F.; Dosche, C.; Dworzak, A.; Oezaslan, M.; Simonsen, S. B.; Kuhn, L. T.; Arenz, M. The Oxygen Reduction Reaction on Pt: Why Particle Size and Interparticle Distance Matter. *ACS Catal.* **2021**, *11* (12), 7144−7153.
(50) Karazhanov, S. Z.; Ravindran, P.; Vajeeston, P.; Ulyashin, A.; Finstad, T. G.; Fjellvåg, H. Phase stability, electronic structure, and optical properties of indium oxide polytypes. *Phys. Rev. B* **2007**, *76* (7), 075129.
(51) Schneider, S. J.; Waring, J. L.; Tressler, R. E. Phase Relations Between Iridium and the Sesquioxides in Air. *J. Res. Natl. Bur Stand A Phys. Chem.* **1965**, *69A* (3), 245−254.
(52) Reier, T.; Oezaslan, M.; Strasser, P. Electrocatalytic Oxygen Evolution Reaction (OER) on Ru, Ir, and Pt Catalysts: A Comparative Study of Nanoparticles and Bulk Materials. *ACS Catal.* **2012**, *2* (8), 1765−1772.
(53) Minguzzi, A.; Locatelli, C.; Lugaresi, O.; Achilli, E.; Cappelletti, G.; Scavini, M.; Coduri, M.; Masala, P.; Sacchi, B.; Vertova, A.; et al. Easy Accommodation of Different Oxidation States in Iridium Oxide Nanoparticles with Different Hydration Degree as Water Oxidation Electrocatalysts. *ACS Catal.* **2015**, *5* (9), 5104−5115.
(54) Fabbri, E.; Taylor, S.; Rabis, A.; Levecque, P.; Conrad, O.; Kötz, R.; Schmidt, T. J. The Effect of Platinum Nanoparticle Distribution on Oxygen Electroreduction Activity and Selectivity. *ChemCatChem.* **2014**, *6* (5), 1122.
(55) Zagalskaya, A.; Alexandrov, V. Mechanistic Study of IrO2 Dissolution during the Electrocatalytic Oxygen Evolution Reaction. *J. Phys. Chem. Lett.* **2020**, *11* (7), 2695−2700.
(56) Danilovic, N.; Subbaraman, R.; Chang, K.-C.; Chang, S. H.; Kang, Y. J.; Snyder, J.; Paulikas, A. P.; Strmcnik, D.; Kim, Y.-T.; Myers, D.; et al. Activity−Stability Trends for the Oxygen Evolution Reaction on Monometallic Oxides in Acidic Environments. *J. Phys. Chem. Lett.* **2014**, *5* (14), 2474−2478.

https://doi.org/10.1021/acs.jpcc.2c06501
J. Phys. Chem. C 2023, 127, 894−906